BIOCHEMISTRY
including biophysical chemistry & molecular biology

Article

pubs.acs.org/biochemistry

# Amphiphilic Residues 29−44 of DREAM N-Termini Mediate Calmodulin:DREAM Complex Formation

Walter G. Gonzalez,[†] Andres S. Arango,[‡] and Jaroslava Miksovska*,[†]

[†]Department of Chemistry and Biochemistry, Florida International University, Miami, Florida 33199, United States
[‡]Department of Physics, Florida International University, Miami, Florida 33199, United States

Supporting Information

**ABSTRACT:** DREAM (downstream regulatory element antagonist modulator) is a neuronal calcium sensor that has been shown to modulate gene expression as well as to be involved in numerous neuronal processes. In this report, we show that association of calcium-bound calmodulin (CaM) with DREAM is mediated by a short amphipathic amino acid sequence located between residues 29 and 44 on DREAM. The association of CaM with a peptide analogous to DREAM(29−44) or to full-length DREAM protein is calcium-dependent with a dissociation constant of 136 nM or 3.4 $\mu$M, respectively. Thermodynamic and kinetic studies show that the observed decrease in affinity for the native protein is due to electrostatic interactions between the basic N-terminus and an electronegative surface on DREAM. These results are further supported by circular dichroism, binding studies, and molecular dynamics simulations. Additionally, fluorescence anisotropy decay measurements show a rotational correlation time of 10.8 ns for a complex of CaM with a DREAM(29−44) peptide, supporting a wraparound semispherical model with 1:1 stoichiometry. Furthermore, the interaction between an IEDANS-labeled CaM construct with DREAM is best modeled as a heterotetramer that adopts an elongated conformation with a correlation time of 45 ns in the presence of $Ca^{2+}$. We also demonstrate that association of CaM with DREAM eliminates the nonspecific interaction of DREAM with the DRE double-stranded DNA sequence of the human *prodynorphin* gene. This work provides molecular insight into the CaM:DREAM complex and its potential role in modulation of gene expression.

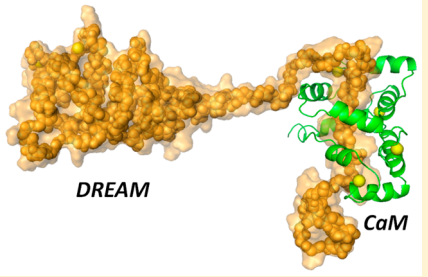


Among the many biological signaling mechanisms, ion−protein and protein−protein interactions play leading roles. Of important relevance is the metal ion calcium ($Ca^{2+}$) and its interaction with calcium binding proteins. Calcium is involved in the regulation of numerous cellular processes such as apoptosis, muscle contraction, neuronal signaling, and cell proliferation, to name a few.[1,2] The role of calcium as an essential messenger highlights the need to understand how calcium binding proteins are able to translate this chemical signal into a biological response. Therefore, understanding the mechanism by which calcium interacts with calcium binding proteins and how these proteins interact with their cellular partners is relevant to discerning the pathology of calcium-related diseases.

One of the most widely studied calcium binding proteins is calmodulin (CaM), a small and ubiquitous (148 residues) acidic protein, with four active EF-hand motifs that can bind calcium with affinities between 1 and 10 $\mu$M.[3] The structure of calcium-bound CaM has been shown to follow a dumbbell arrangement of the N- and C-terminal domain, while removal of calcium induces local rearrangement of the EF-hands and an increase in the flexibility of the N- and C-termini.[4,5] The interaction of CaM with proteins as well as with their peptide fragments often surpasses the affinity for calcium.[6] The mechanism of calcium-induced protein binding to CaM can be simplified as a calcium-triggered exposure of hydrophobic surfaces, which facilitates the association of the target protein. The protein fragments involved in CaM association often function as an autoinhibitory domain or are directly involved in protein activity. These CaM recognition sequences are amphipathic in nature with numerous positive and bulky hydrophobic residues forming electrostatic and hydrophobic contacts. CaM binding sequences can be grouped by those that are enhanced by calcium or are calcium-independent.[6] The fact that CaM has been shown to constitute ∼0.1% of total cytosolic protein also highlights the role of this signal transducer in calcium signaling.[7]

A relatively new member of the group of EF-hand calcium binding proteins is the downstream regulatory element antagonist modulator (DREAM), which has been shown to be one of the first proteins to regulate gene expression in a calcium-dependent manner.[8] Additionally, this protein was identified to be involved in presenilin fragmentation,[9] as well as regulation of the $K_V4$ subfamily of voltage-gated potassium channels.[10] DREAM is a 256-amino acid, 29 kDa protein highly expressed in the brain[10] and belongs to the superfamily of neuronal calcium sensors (NCS) that are highly homologous to NCS-1 and recoverin.[11] Like other NCS, DREAM contains four EF-hand motifs. EF-hand 1 is unable to bind calcium. EF-hand 2 binds preferentially magnesium, and the two EF-hands at the C-

**Received:** March 8, 2015
**Revised:** June 15, 2015
**Published:** June 25, 2015





DOI: 10.1021/acs.biochem.5b00251
*Biochemistry* 2015, 54, 4391−4403

terminus bind calcium with affinities between 1 and 10 $\mu$M.[12] Three other proteins closely homologous to DREAM (KChIP1, KChIP2, and KChIP4) have also been identified and together form the KChIP subgroup of NCS proteins.[10] Despite the high degree of homology of KChIPs at their C-termini, the N-terminal region and tissue expression are highly divergent.

A recent report by Ramachandran and co-workers showed that DREAM and CaM form a complex and enhance the activation of calcineurin.[13] Additionally, more than 40 protein partners were identified to interact with DREAM in a calcium-dependent and -independent manner, further highlighting the role of DREAM as a calcium sensor involved in numerous cell processes.[13] Consequently, given the wide spectrum of processes regulated by CaM and the multifunctional activity of DREAM, a better understanding of the molecular mechanism by which these two proteins interact and how such interaction can be inhibited is necessary to further explore the biological significance of this protein complex.

Numerous studies have addressed the molecular structure of DREAM and how calcium-induced changes are translated into regulation of protein−protein and protein−DNA interactions.[13−15] Nuclear magnetic resonance (NMR) structures of the calcium binding C-terminal domain [EF-hand 3 and EF-hand 4, residues 161−256, Protein Data Bank (PDB) entry 2E6W][16] and of the core domain (EF-hands 1−4, residues 76−256, PDB entry 2JUL)[15] have been resolved. Interestingly, DREAM has been shown to be cleaved at Asp61−Asp64 by caspase-3, which indicates that inside the cell there may be a subpopulation DREAM with a structure analogous to that resolved by NMR.[17] However, no model for the full-length DREAM protein is currently available.

In this report, we seek to identify the amino acid sequence at the N-terminus of DREAM involved in CaM binding. We further characterize the secondary and tertiary structure of the DREAM N-terminus using a combination of theoretical and experimental techniques to build a molecular model for the full-length protein. Finally, we propose a mechanism by which CaM associates with DREAM and sequesters its N-terminal domain, which could potentially modulate DREAM's interaction with binding targets. Altogether, the results presented here provide us with a molecular understanding of the CaM:DREAM interaction and underline the implication of this protein complex in calcium signaling and gene expression. Some of these results have been previously presented in abstract forms.[18,19]

## MATERIALS AND METHODS

**General.** NS5806 {1-[2,4-dibromo-6-(1*H*-tetrazol-5-yl)-phenyl]-3-[3,5-bis(trifluoromethyl)phenyl]urea} at >99% purity was purchased from Tocris Bioscience. Trifluoperazine (TFP) was purchased from Sigma-Aldrich. 1,8-ANS (8-anilino-1-naphthalenesulfonic acid) was purchased from Cayman Chemical Co. 1,5-IAEDANS and rhodamine red C2 maleimide were purchased from Invitrogen. A concentrated stock solution of NS5806 was prepared by dissolving NS5806 in DMSO and stored at −20 °C. Concentrated TFP and 1,8-ANS stocks were prepared in ultrapure (18.2 MΩ) water. The concentrations of NS5806, TFP, and 1,8-ANS stocks were determined spectrophotometrically using an $\varepsilon_{295}$ of 2200 $M^{-1}$ $cm^{-1}$ for NS5806 in 20 mM MOPS (pH 7.4), an $\varepsilon_{306}$ of 3300 $M^{-1}$ $cm^{-1}$ for TFP, and an $\varepsilon_{350}$ of 4995 $M^{-1}$ $cm^{-1}$ for 1,8-ANS in water.

**Isolation and Purification of DREAM Constructs.** The recombinant mouse DREAM(Δ64) construct was expressed in *Escherichia coli* BL21(DE3) cells and purified according to previously published procedures.[14,20] Rat calmodulin (herein termed CaM) plasmid was a kind gift from J. P. Davis (The Ohio State University, Columbus, OH) that was subcloned in BL21(DE3) cells and purified as previously described.[21] A CaM(A148C) mutant was obtained by site-directed mutagenesis of the CaM plasmid using the QuickChange Lightning kit (Agilent Technologies, Palo Alto, CA) and confirmed by DNA sequencing (Eurofins Genomics). Following a CaM and DREAM co-expression protocol at a low temperature, we have been able to recover milligram quantities of soluble full-length DREAM. *E. coli* BL21(DE3) competent cells were transformed with CaM and DREAM plasmids and grown in LB medium at 37 °C in the presence of 100 $\mu$g/mL ampicillin until an optical density of 2 at 600 nm was reached. The medium was then quickly chilled on an ice bath to 4 °C, and protein expression was induced by adding 0.2 mM IPTG. The medium was placed back in the shaker at 250 rpm for an additional 6 h at 18 °C, and cells were harvested by centrifugation. The cell pellet was resuspended in 100 mM Tris buffer (pH 8.0), 0.5 M NaCl, 1 mM $CaCl_2$, 5 mM $MgCl_2$, 5 mM imidazole, 1.0% Triton X-100, 0.5% Tween 20 supplemented with 20 $\mu$g/mL DNase, 200 $\mu$g/mL lysozyme, and 0.5 mM phenylmethanesulfonyl fluoride and sonicated on an ice bath for 30 cycles at 30% duty cycle. The cell lysate was centrifuged at 11000*g* for 50 min, and the supernatant was loaded on a Ni-NTA column equilibrated with buffer A [20 mM Tris (pH 7.4), 300 mM NaCl, 0.5 mM $CaCl_2$, and 10 mM LDAO]. DREAM was washed extensively with buffer A and eluted in buffer B [20 mM Tris (pH 7.4) and 10 mM LDAO] supplemented with 250 mM imidazole. Selected fractions were loaded onto a DEAE-sepharose anion exchange column previously equilibrated with buffer B, washed with buffer B and 80 mM NaCl, and then eluted with 180 mM NaCl; the final protein was stored in 5 mM Tris (pH 8.0). The purity of all protein constructs was assessed using sodium dodecyl sulfate−polyacrylamide gel electrophoresis, while secondary structure and tertiary structure were confirmed using the known far-UV CD transition and tryptophan fluorescence change upon calcium binding.

**Protein Labeling and Sample Preparation.** Labeling of CaM(A148C) with 1,5-IAEDANS or rhodamine red C2 (RRC2) maleimide was conducted after reduction of cysteine residues with 5 mM TCEP in 200 mM Tris (pH 7.4) followed by extensive purging with argon and addition of (10−50-fold) excess fluorophore freshly prepared in DMF. The reaction was allowed to proceed for 24 h at 4 °C while the mixture was being constantly stirred in the dark. Unbound fluorophore was removed by size exclusion chromatography through a Sephadex G10 column. Labeled protein fractions were selected on the basis of their absorption and fluorescence anisotropy and extensively dialyzed in 5 mM Tris (pH 7.4). The fraction of labeled protein was determined by dividing the fluorophore concentration (1,5-IAEDANS $\varepsilon_{336}$ = 6100 $M^{-1}$ $cm^{-1}$ in buffer,[22] or RRC2 $\varepsilon_{560}$ = 119000 $M^{-1}$ $cm^{-1}$ in DMSO) by the protein concentration [CaM(A148C) $\varepsilon_{280}$ = 3140 $M^{-1}$ $cm^{-1}$] after correction by the absorption of the fluorophore at 280 nm. Protein samples were prepared by dilution, and the final protein concentration was measured using an $\varepsilon_{280}$ of 31200 $M^{-1}$ $cm^{-1}$ for DREAM and an $\varepsilon_{280}$ of 19000 $M^{-1}$ $cm^{-1}$ for DREAM(Δ64). The extrinsic fluorophore 1,8-ANS was added to protein samples directly from a concentrated stock. Calcium was added at a 10-fold excess for DREAM and 1 mM for DRE29 samples, while 2 mM EDTA was used to remove calcium; 50 mM $CaCl_2$ and 200 mM EDTA standard stocks at pH 7.4 were used. CaM labeled with


DOI: 10.1021/acs.biochem.5b00251
*Biochemistry* 2015, 54, 4391−4403

IAEDANS or RRC2 is termed CaM-IAEDANS or CaMRR2, respectively.

**Steady-State Fluorescence Measurements.** Fluorescence emission measurements were taken using a custom PC1 spectrofluorimeter (ISS, Champaign, IL). Tryptophan emission spectra were measured using 295 nm excitation, and titrations were conducted in a 0.2 cm × 1 cm path-length quartz cuvette with excitation along the 0.2 cm path. The dissociation constants for binding of CaM to DREAM were determined by a nonlinear fit of the change in normalized fluorescence emission spectra at 370 nm using a single-binding site model:

$$\Delta F = \frac{K_d + nP_t + L_t - \sqrt{(K_d + nP_t + L_t)^2 - 4nP_tL_t}}{2c} \quad (1)$$

where $\Delta F$ is the intensity change, $K_d$ is the dissociation constant, $n$ is the number of binding sites, $P_t$ is the total protein concentration, $L_t$ is the total ligand concentration, and $c$ is a proportionality constant. Emission intensities were corrected for dilution effects and the inner filter effect.

To study the interaction between CaM and the N-terminus of DREAM, we employed a fluorescently labeled peptide homologous to DREAM(29−44), and the fluorescence anisotropy increase upon complex formation was used to determine the affinity. A peptide homologous to DREAM(29−44) with a FITC label at the N-terminus was purchased from ThinkPeptides. Additional titrations of apo and $Ca^{2+}$CaMRR2 and DREAM(29−44)-FITC peptides were conducted by monitoring the quenching of FITC fluorescence by rhodamine through energy transfer. Equation 1 was used for fitting of the anisotropy and quenching data, where $\Delta F$ represents the change in anisotropy or intensity.

The effect of CaM on the interaction of DREAM with the DRE sequence of human prodynorphin was probed by steady-state fluorescence anisotropy. A synthetic oligonucleotide corresponding to the DRE sequence 5′-GAAGCCGGAGTCAAGGAGGCCCCTG-3′ labeled at the 5′ end with FITC was purchased (Eurofins) and used without further purification, and the complementary strand was not labeled. Samples were prepared as previously reported.[12]

**Circular Dichroism (CD) Measurements.** All CD spectra were measured using a Jasco J-810 CD spectropolarimeter. The far-UV CD spectra were measured at a protein concentration of 10 $\mu$M through a 1 mm path in 5 mM phosphate buffer (pH 7.4). Near-UV CD spectra were measured along a 1 mm path using 160 $\mu$M DREAM and 560 $\mu$M DREAM(Δ64) in 20 mM Tris (pH 7.4) and 10 mM LDAO. All measurements were conducted at 16 °C, and traces represent an average of 20 scans.

**Stopped-Flow Kinetics.** A PC1 spectrofluorometer (ISS) with an SFA-20 stopped-flow kinetics accessory (Hi-Tech, Salisbury, U.K.) was used to determine the dissociation rate constants by monitoring the change in anisotropy upon complex dissociation. Experiments with CaM and DREAM(29−44)-FITC, as well as CaMRR2 and DREAM, were conducted by mixing a 1:1 volumetric ratio of the protein complexes in the presence of 100 $\mu$M calcium with 2 mM EDTA in 20 mM Tris (pH 7.4). Samples were excited using 470 nm excitation for DREAM(29−44)-FITC and 520 nm excitation for CaMRR2. The change in fluorescence anisotropy upon complex dissociation was determined by collecting the fluorescence at 520 ± 10 nm for FITC and 600 ± 10 nm for RRC2 using a T-format configuration. The dissociation of $Ca^{2+}$ from CaM was monitored using 285 nm excitation and the intrinsic tyrosine fluorescence in the L-format through a 305 nm long pass filter. The temperature was controlled using a circulating water bath (Fisher, Isotemp M9100) and measured at the sample holder to ±0.5 °C. Dissociation kinetic data were best fitted by single- or double-exponential decay equations using Origin version 8.0 (OriginLab Corp.).

**Fluorescence Lifetime and Anisotropy Decay Measurements.** Fluorescence decay data were obtained using a ChronosFD spectrofluorometer (ISS) in the frequency domain mode. The fluorescence decay lifetime of IAEDANS or FITC complexes was determined by excitation with a 370 or 470 nm modulated laser diode, respectively. Fluorescence was collected through a 400 nm long pass filter for IAEDANS samples or a 500 nm long pass filter for FITC samples. POPOP [1,4-bis(5-phenyloxazol-2-yl)benzene] in ethanol ($\tau$ = 1.35 ns) or rhodamine B in water ($\tau$ = 1.70 ns) was used as a lifetime reference; polarizers were set at the magic angle configuration. Anisotropy decay measurements were conducted under identical conditions. Modulation-phase data were fitted using GlobalsWE software, and the $\chi^2$ parameter was used as a criterion for goodness of fit.[23]

**Molecular Modeling and Dynamic Simulations.** The initial structure of $Ca^{2+}$-bound DREAM(76−256) (PDB entry 2JUL, conformation 1) was employed as a starting model of the core domain of the full-length protein.[15] The secondary structure of the N-terminal residues of DREAM not resolved in the NMR structure and those comprising helix 1 (residues 76−86) were predicted by a combination of six secondary structure prediction software algorithms. To decrease the variability of the helix prediction, a helical conformation was only accepted if it was predicted by at least four of the algorithms. A model for the full-length protein was constructed by modeling the first 90 residues as an extended helix or loop based on the secondary structure prediction followed by a 10 ns molecular dynamics simulation to equilibrate the structure. The helical structure of residues 76−86 (helix 1) was used to align the peptide to the published NMR structure to obtain the structure of DREAM from residue 1 to 256.

The DREAM model was solvated and ionized as described below (122639 atoms) followed by classical and accelerated molecular dynamics simulations (cMD and aMD, respectively) to identify the dynamics and folding of the N-terminus. The parameters for the aMD were determined from the total energy and dihedral energy from a cMD simulation ($\langle E_{total} \rangle$ = −330141.1 kcal/mol, and $\langle E_{dihed} \rangle$ = 973.1 kcal/mol). The dihedral boost was applied above a threshold energy set to 1993.1 kcal/mol with a dihedral $\alpha$ value of 204 kcal/mol. All-atom explicit solvent molecular dynamics simulations were obtained using the molecular dynamics simulation package NAMD[24] with the CHARMM27 force fields.[25] All simulated systems were solvated in a periodic TIP3P water box with 10 Å margins and ionized with 150 mM NaCl.[26] Long range interactions were treated with the PME method[27] with a 12 Å cutoff. Energy was minimized with a conjugate gradient algorithm, followed by heating at 1 K/ps from 0 to 310 K. After a temperature of 310 K had been reached, a 100 ps equilibration step in the *NVT* ensemble using Langevin dynamics with a 1 fs integration time was conducted. Production runs were in the *NPT* ensemble (1 atm and 310 K) both with Langevin coupling and with a 2 fs integration time. All simulations were performed on an i7-4770/GTX-780Ti system using NAMD 2.09. Trajectory files were saved every 20 ps for further analysis. The initial structure used for cMD and aMD in the absence of $Ca^{2+}$ was modeled as coarse



DOI: 10.1021/acs.biochem.5b00251
*Biochemistry* 2015, 54, 4391−4403

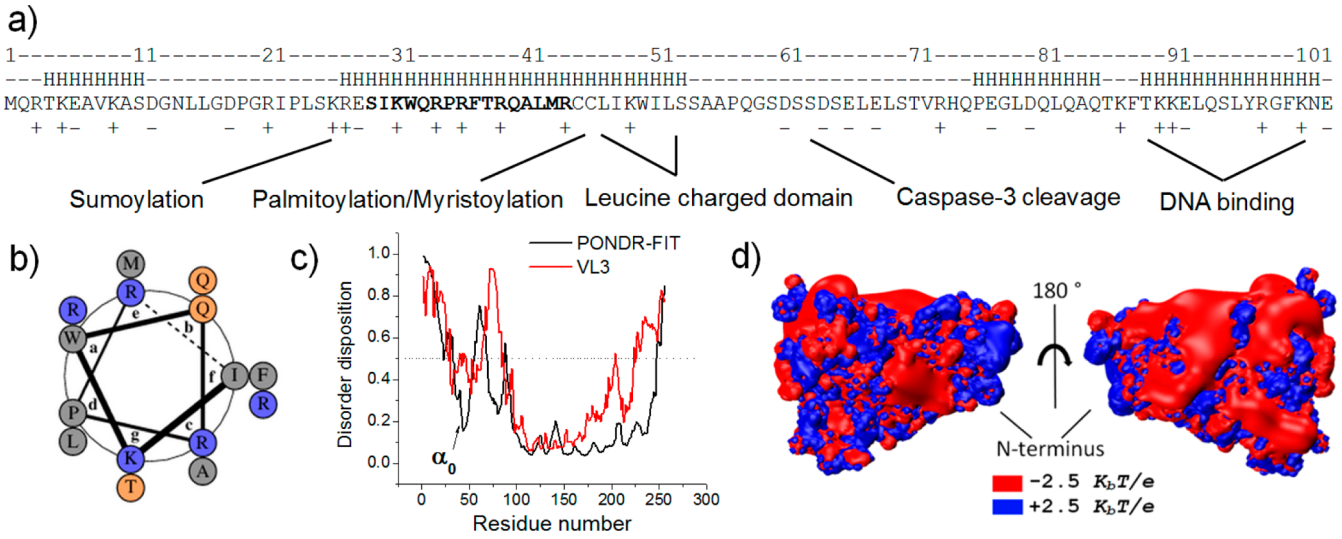


**Figure 1.** (a) Bioinformatics analysis of the first 100 residues at the N-terminus of mouse DREAM, indicating regions of helical structure and charge distribution. Proposed sites for posttranslational modification and ligand interactions are shown. (b) Helical plot analysis of residues 29−44 of DREAM. (c) DREAM amino acid sequence disorder prediction using the PONDR-FIT and VL3 prediction servers.[37,38] (d) Potential energy surface of apoDREAM (lacking the first 77 residues) calculated using the published NMR structure[15] and the APBS plugin of the VMD software with CHARMM parameters at a mobile ion concentration of 150 mM.[26,57]

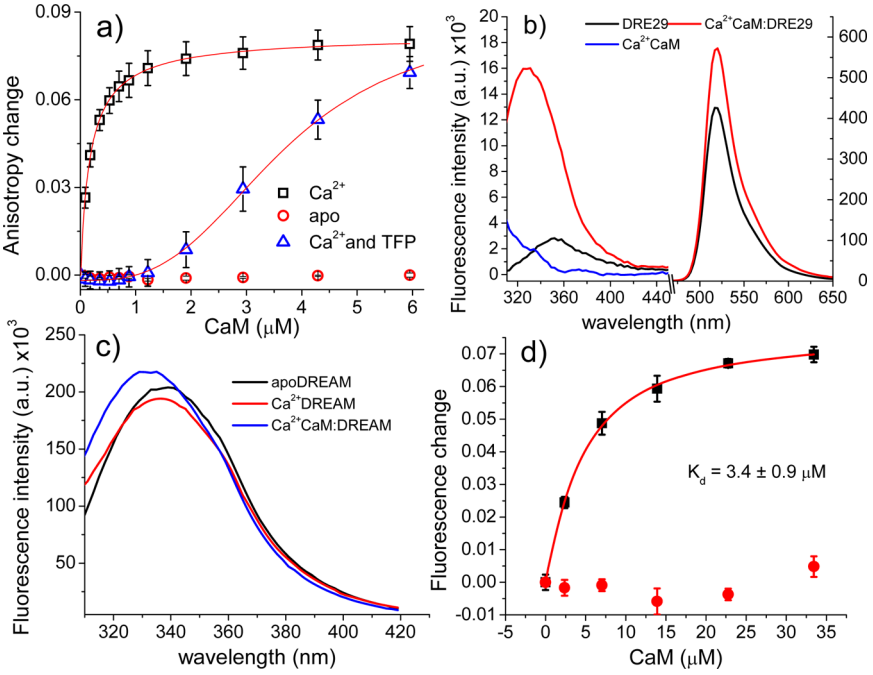


**Figure 2.** Titration curves for binding of calmodulin to (a) 100 nM FITC-labeled peptide analogous to residues 29−44 of mouse DREAM (DRE29) in the absence (circles) or presence (squares) of 1 mM calcium ($K_d$ = 136 ± 10 nM) and in the presence of calcium and 30 $\mu$M trifluoperazine (triangles). (b) Fluorescence emission spectra of 5 $\mu$M DRE29 peptide in the presence or absence of 10 $\mu$M $Ca^{2+}$CaM. The sample was excited at 300 ± 4 nm, which resulted in a negligible contribution from tyrosine on CaM. Buffer background emission was subtracted to decrease Rayleigh, Raman, and second harmonic peaks contributing to the signal. (c) Observed shift and increase in tryptophan fluorescence upon calmodulin binding. (d) Normalized tryptophan fluorescence change at 370 nm of DREAM(1−256) upon addition of calmodulin in the absence (circles) and presence (squares) or 1 mM calcium ($K_d$ = 3.4 ± 0.9 $\mu$M).

grained spheres using the VMD plugin and MARTINI parameters.[28] The structure was minimized, and simulations were run in the *NPT* ensemble. Solvation, ionization, and force field parameters were identical to those utilized in cMD and aMD simulations, but with an increased time step of 20 fs.

## RESULTS

**Calmodulin Stabilizes the N-Terminus of DREAM and Increases the Solubility of the Protein Complex.** Previous reports have shown that DREAM readily forms inclusion bodies when it is overexpressed in BL21(DE3) *E. coli* cells, whereas DREAM(Δ64) was recovered in moderate yields as a soluble protein,[14,15] indicating that residues 1−64 of DREAM destabilize



DOI: 10.1021/acs.biochem.5b00251
*Biochemistry* 2015, 54, 4391−4403

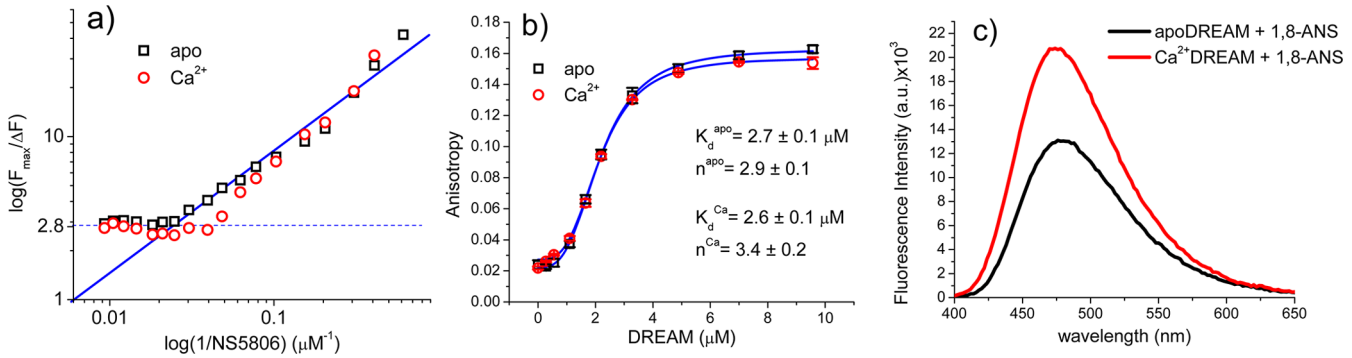


**Figure 3.** (a) Modified Stern−Volmer analysis of tryptophan fluorescence quenching upon binding of NS5806 to apo and $Ca^{2+}$DREAM. Solid lines illustrate the expected traces for complete quenching, and dashed lines show the intercept at 2.83 ± 0.12. (b) Association of Kv4.3(1−22)-FITC with apo and $Ca^{2+}$DREAM monitored using fluorescence anisotropy. Solid lines represent the best fit to the data using a Hill binding model with the recovered parameters shown in the inset. (c) Fluorescence spectra of 1,8-ANS bound to apoDREAM with a $\lambda_{max}$ of 478 nm and $Ca^{2+}$DREAM with a $\lambda_{max}$ of 475 nm. These results support the idea that the accessibility of the hydrophobic cavity at the C-terminus of DREAM is not compromised by the presence of N-terminal residues 1−65.

the protein under conditions used for recombinant protein expression. It has also been shown that the association between DREAM and CaM is mediated by an amino acid sequence within the 94 N-terminal residues of DREAM.[13] We hypothesized that binding of CaM could stabilize DREAM and lead to an increase in solubility during recombinant expression. To test this hypothesis, we co-expressed CaM and DREAM in BL21(DE3) *E. coli* at low temperatures (see Materials and Methods). Under such conditions, DREAM was recovered as a soluble protein with yields of ∼40 mg. Interestingly, we have observed that 10 mM LDAO abolishes the CaM:DREAM interaction and prevents DREAM aggregation in the presence of saturating calcium, which facilitates the purification of soluble DREAM. We envision this protocol being more robust than the previously employed method of inclusion body refolding[14] or GST fusion tags.[13] These results support the role of CaM as a protein cofactor that stabilizes the N-terminus of DREAM and potentially facilitates its translocation in the cell.

**Residues 29−44 at the N-Terminus of DREAM Mediate CaM Binding in a Calcium-Dependent Manner.** Bioinformatics analysis of the N-terminus of DREAM revealed the presence of numerous basic, acidic, and hydrophobic residues. Of particular interest is a short amphipathic 16-residue peptide segment (residues 29−44, SIKWQRPRFTRQALMR) with a high density of positively charged residues and hydrophobic residues (Figure 1). This short amino acid sequence is quite similar to the 1−8−14 type A binding motif associated with other calmodulin binding peptides,[6] with a total charge of +5 and bulky hydrophobic residues Ile30, Trp32, Phe37, Leu42, and Met43. Secondary structure prediction also shows this sequence to have a moderate helical propensity. The helical wheel diagram of DREAM(29−44) shows an arrangement of dispersed positive and hydrophobic residues (Figure 1b). This small helical region is surrounded by extended disordered domains (Figure 1c), which may enhance the flexibility of the N-terminus. The core domain of DREAM (residues 76−256) exhibits a strong electronegative surface opposite a hydrophobic groove that has been shown to be involved in ligand binding[20,29] (Figure 1d).

Calmodulin is well-known to bind positively charged amphipathic protein segments in a calcium-dependent manner; therefore, we hypothesize that a similar binding mechanism is present in DREAM. To test this hypothesis, we studied binding of CaM to a fluorescently labeled peptide homologous to residues 29−44 of DREAM (herein named DRE29). Upon addition of calcium-bound CaM to DRE29, a large increase in fluorescence anisotropy was measured, indicative of binding. The binding curves show a clear calcium-dependent binding of the DRE29 peptide to calmodulin, with a dissociation constant ($K_d$) in the calcium-bound form of 136 ± 10 nM and negligible binding in the absence of calcium (Figure 2a). Similar results were obtained using FRET experiments between DRE29 and CaMRR2, with a dissociation constant of 132 ± 16 nM (Figure S1a,b of the Supporting Information). The binding of CaM to DRE29 was inhibited in the presence of the antipsychotic drug and known calmodulin inhibitor trifluoperazine (TFP). Analysis of the binding using a competitive model in the presence of 30 μM TFP, using the reported affinity of TFP for CaM of 1 μM,[30] shows that a single bound TFP is sufficient to inhibit binding of the peptide (Figure S1c of the Supporting Information). Because the higher-affinity binding sites of TFP on CaM are at the C-terminal domain, the data show that this domain is mainly responsible for binding the DRE29 peptide.[31]

The emission spectra of DRE29 in the presence or absence of $Ca^{2+}$CaM show two peaks corresponding to Trp32 and FITC (Figure 2b). The weak fluorescence of Trp32 is due to an efficient energy transfer to the FITC label; however, upon association with CaM, an increase in fluorescence and a blue shift from 351 to 329 nm are observed. The increase in FITC emission is expected on the basis of the increase in the quantum yield of Trp32. It is also possible that restructuring of the DRE29 peptide in the CaM:DRE29 complex increases the energy transfer efficiency. Overall, these results identify the amphipathic region in the N-terminus of DREAM spanning residues 29−44 as mediating the calcium-dependent binding of CaM. It also shows that upon association with $Ca^{2+}$CaM the solvent accessibility of Trp32 decreases.

**The N-Terminal Domain of DREAM Does Not Block Its Hydrophobic Cavity.** The intrinsic tryptophan fluorescence of DREAM decreases upon calcium binding, a transition similar to that observed for DREAM(Δ64).[8,32] Upon association of $Ca^{2+}$CaM with DREAM, a 5 nm blue shift from 337 to 332 nm is observed along with an increase in fluorescence intensity (Figure 2c). As in our peptide studies, CaM interacts with DREAM only in the presence of calcium ($K_d$ = 3.4 ± 0.9 μM), with no detectable interaction in the absence of $Ca^{2+}$ (Figure 2d), in good agreement with the previously reported value of 3 μM.[13] The decreased affinity of CaM for the N-terminus of DREAM compared to the affinity of isolated residues 29−44 may indicate


DOI: 10.1021/acs.biochem.5b00251
*Biochemistry* 2015, 54, 4391−4403

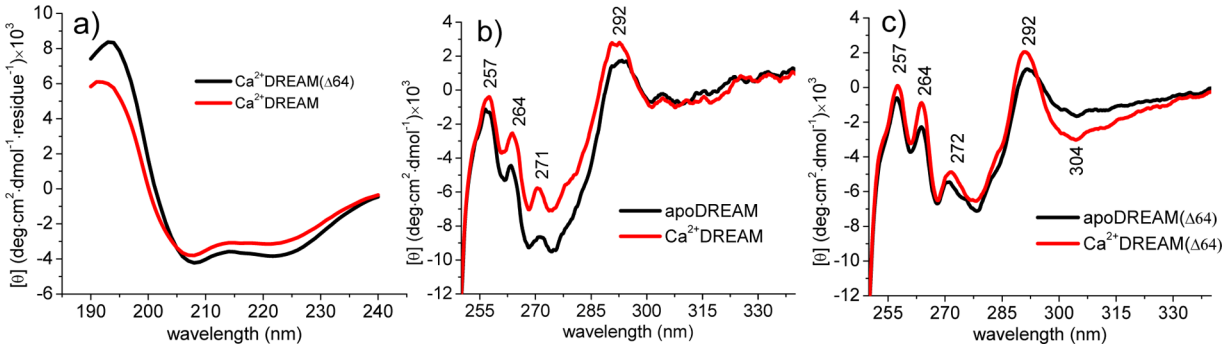


**Figure 4.** (a) Far-UV CD spectra of DREAM(Δ64) and DREAM in the presence of 100 $\mu$M calcium in 5 mM phosphate buffer (pH 7.4). Near-UV CD spectra of (b) DREAM(Δ64) and (c) DREAM in the absence and presence of calcium.

that the N-terminus is not completely solvent accessible. This could be easily explained by a model in which the N-terminus collapses on the DREAM core domain (residues 76−256) and reduces the affinity of CaM. Indeed, a similar folding was observed in the structure of calcium-bound KChIP4 and $Mg^{2+}$-bound caldendrin.[33,34] Therefore, to test whether the N-terminus of DREAM (residues 29−44) physically interacts with the core domain, we conducted titrations of DRE29 with DREAM(Δ64). We observe an interaction between DRE29 and DREAM(Δ64) with a $K_d$ of ∼30 $\mu$M; however, a similar affinity with DREAM was observed (Figure S2 of the Supporting Information). In the presence of 100 mM NaCl, the affinity of the DRE29 peptide with DREAM(Δ64) decreased to a $K_d$ of ∼0.3 mM. These results indicate that the observed association between residues 29−44 and the core domain of DREAM is nonspecific and mediated by electrostatic interactions.

DREAM(Δ64) protein has been shown to interact with small hydrophobic ligands such as arachidonic acid, the $K^+$ current activator NS5806, and the hydrophobic probes 1,8-ANS and 2,6-ANS.[20,29] These ligands associate with a hydrophobic cavity at the C-terminus of DREAM whose accessibility increases upon association of $Ca^{2+}$ with EF-3 and EF-4. Association of the hydrophobic N-terminus of $K_V4$ channels with DREAM and other KChIPs is also mediated by a hydrophobic groove that extends from the C- to N-terminus.[20,35,36] Therefore, we investigated whether the presence of residues 1−64 in DREAM can affect the binding of these hydrophobic ligands. Titrations of a peptide homologous to the hydrophobic N-terminus of Kv4.3 (residues 2−22) show that the affinity is not only independent of calcium but also identical to the previously reported value for binding to the $Ca^{2+}$-bound DREAM(Δ64) construct (Figure 3).[20] Similarly, the hydrophobic probe 1,8-ANS and NS5806 compound showed interactions with DREAM that are similar to those observed for DREAM(Δ64).[20,29] These results support the idea that the N-terminus of DREAM does not function as an autoinhibitory domain of the hydrophobic cavity as observed for isoform 4 of KChIP4.[33] Analysis of the NS5806 tryptophan quenching data using a modified Stern−Volmer plot shows that unlike DREAM(Δ64), where Trp169 is completely quenched,[20] only one of three tryptophans is quenched in DREAM (Figure 3a). This observation can easily be explained if the N-terminus of DREAM is not near the hydrophobic C-terminus where the Kv4.3 N-terminus, 1,8-ANS, or NS5806 binds or if the association of the hydrophobic ligand induces the displacement of the N-terminus.

**Calcium Binding to DREAM Induces a Structural Rearrangement at the N-Terminus.** The structure of the N-terminus of DREAM (residues 1−75) has not been resolved, and on the basis of NMR results, it has been proposed to form a random coil.[15] To improve our understanding of the mechanism of CaM binding, we set forth to identify the potential secondary structure of the N-terminal residues of DREAM using structure prediction tools and CD. The N-terminus of DREAM shows the potential formation of two $\alpha$ helices between residues 4 and 11 and between residues 27 and 53, herein named $\alpha_{-1}$ and $\alpha_0$, respectively (Figure 1). Two additional $\alpha$ helices comprising residues 76−85 and 88−102 were also identified; these helices correspond to $\alpha_1$ and $\alpha_2$ previously identified by NMR.[15] Further analysis of the N-terminus of DREAM using protein disorder prediction tools also shows residues surrounding $\alpha_0$ as having a strong propensity to form disordered regions.[37,38] Molecular dynamics simulations support the idea that both N-terminal helices retain their secondary structure and are flexible relative to each other (Figure S3 of the Supporting Information), with $\alpha_0$ showing an expected bend at Pro36. Overall, these bioinformatics analyses and simulations of the N-terminal domain of DREAM indicate that this domain forms a disordered region with a small helical structure connected to the core of DREAM by a 21-residue disordered region rich in small hydrophilic residues (residues 54−75).

To gain insight into the secondary structure of DREAM and its N-terminus, we also performed near- and far-UV circular dichroism measurements on DREAM and DREAM(Δ64). The far-UV CD signal for both constructs shows the characteristic spectra of $\alpha$-helical proteins, with negative peaks at 220 and 207 nm and a larger positive peak near 190 nm (Figure 4a). The magnitude of the CD signal was dependent on $Ca^{2+}$ for both constructs with an increase in the 190 nm peak and a decrease in 220/207 nm peaks upon calcium binding (data not shown). However, the magnitude of the positive and negative peaks of DREAM in the absence or presence of calcium was smaller than that of DREAM(Δ64), indicative of there being less $\alpha$-helical content in the full-length construct. Analysis of the far-UV CD spectra with the K2D secondary structure prediction tools shows $\alpha$-helical contents of 68 and 50% for calcium-bound DREAM(Δ64) and DREAM, respectively. A fully unfolded N-terminal domain in DREAM would result in a 47% $\alpha$-helical content, which is slightly lower than the value determined here. Therefore, the N-terminal domain of DREAM likely forms a disordered domain with a small region of $\alpha$-helical structure near the CaM binding sequence.

On the other hand, the near-UV CD spectra for both DREAM constructs showed complex and distinct positive and negative peaks. In the absence of calcium, DREAM showed a broad negative band with fine structured positive and negative peaks. The peaks between 256 and 272 nm are likely due to


DOI: 10.1021/acs.biochem.5b00251
*Biochemistry* 2015, 54, 4391−4403

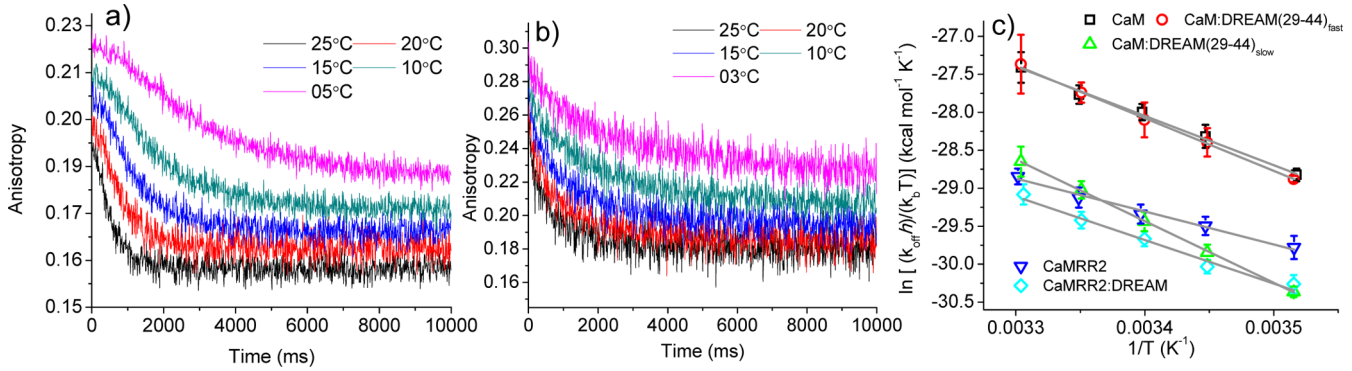


**Figure 5.** Dissociation kinetics of (a) 10 $\mu$M CaM and 1 $\mu$M DRE29 and (b) 1 $\mu$M CaMRR2 and 10 $\mu$M DREAM upon addition of 1 mM EDTA monitored using T-format fluorescence anisotropy as a function of temperature. (c) Eyring plot analysis of the dissociation constant as a function of temperature. Solid lines represent best linear fits to the data.

phenylalanine residues, whereas the peaks between 275 and 305 nm are associated with tyrosine and tryptophan residues.[39,40] Calcium binding resulted in an increase in the ellipticity signal between 256 and 295 nm (Figure 4b), without a significant shift of the observed vibronic structures. The near-UV CD spectra of DREAM(Δ64) in the absence of calcium showed many similarities in terms of its phenylalanine and tyrosine peaks to DREAM, whereas a larger peak at 290 nm was observed in the tryptophan region. Binding of calcium to DREAM(Δ64) did not induce major changes in the spectra, with the exception of a decrease in ellipticity near 305 nm (Figure 4c). The presence of only three additional aromatic residues in DREAM compared to the construct lacking the first 64 residues indicates that the increase in ellipticity between 270 and 290 nm likely arises from Phe37, Trp32, and/or Trp50. Additionally, the broad changes in ellipticity upon binding of calcium in DREAM but not in DREAM(Δ64) indicate that the N-terminal residues undergo a structural rearrangement that restricts the solvent accessibility of Trp32 and/or Trp50.[41] These results support the idea that the conformation of the N-terminal residues of DREAM may be affected by calcium binding.

**The Core Domain of DREAM Facilitates Dissociation of the CaM:DREAM Complex.** To better understand the mechanism of CaM:DREAM interaction, we determined the kinetics of formation of the CaM:DREAM complex by monitoring the fluorescence change of CaM and CaMRR2 upon dissociation from DRE29 and DREAM. Initial attempts to resolve the association rate by mixing a 1:1 volumetric ratio of 10 $\mu$M $Ca^{2+}$CaM and 0.5 $\mu$M DRE29 or 10 $\mu$M apoDREAM and 0.5 $\mu$M CaMRR2 with 1 mM $CaCl_2$ showed that the protein complex was formed within the dead time of our stopped-flow instrument (~20 ms), indicating that like other CaM binding peptides and proteins,[42,43] the bimolecular association rate constant is near the diffusion limit, with $k_{on}$ in excess of $10^8$ $M^{-1}$ $s^{-1}$. Dissociation of $Ca^{2+}$ from 2.5 $\mu$M CaM by 1 mM EDTA monitored using tyrosine fluorescence showed a monophasic decay with a $k_{off}$ of 7.9 ± 0.6 $s^{-1}$ at 25 °C, as previously reported.[42] The dissociation of calcium from 0.5 $\mu$M CaMRR2 determined by monitoring the anisotropy change of the rhodamine label at Cys148 was 4 times slower than that observed for CaM, with a $k_{off}$ of 1.9 ± 0.1 $s^{-1}$ at 25 °C. The slow dissociation of $Ca^{2+}$ from CaMRR2 could be likely due to stabilization of the calcium-exposed hydrophobic cavity at the C-terminus by the rhodamine label or due to measurement of a structural change sequential to calcium dissociation.

On the other hand, mixing of $Ca^{2+}$CaM:DRE29 and $Ca^{2+}$CaMRR2:DREAM complexes with 2 mM EDTA resulted in a well-resolved decrease in fluorescence anisotropy indicative of complex dissociation upon $Ca^{2+}$ removal (Figure 5a,b). The dissociations of CaM:DRE29 and CaMRR2:DREAM complexes were best fitted by double- and single-exponential decay functions, respectively (Table 1). The rates of dissociation

**Table 1. Activation Parameters for CaM:DRE29 and CaMRR2:DREAM Dissociation**

| | $k_{off}$ ($s^{-1}$)[a] | $\Delta H^{‡}$ (kcal/mol) | $T\Delta S^{‡}$ (kcal/mol) |
|---|---|---|---|
| CaM | 7.9 ± 0.6 | 12.9 ± 0.5 | −3.5 ± 0.5 |
| CaM-DRE29$_{fast}$ | 8.3 ± 3.5 | 13.8 ± 0.4 | −2.7 ± 0.2 |
| CaM-DRE29$_{slow}$ | 2.3 ± 0.16 | 16.1 ± 0.3 | −1.1 ± 0.2 |
| CaMRR2 | 1.9 ± 0.1 | 8.6 ± 0.6 | −8.6 ± 0.6 |
| CaMRR2:DREAM[b] | 1.5 ± 0.1 | 13.5 ± 1.2 | −4.0 ± 0.7 |

[a]At 298 K. [b]Activation enthalpy and entropy corrected for the fraction of DREAM bound ($f_b$ = 0.57) based on the concentration of DREAM of 5 $\mu$M and a $K_d$ of 3.3 $\mu$M.

($k_{off}$) of CaM from the DRE29 peptide and DREAM protein were 2.3 ± 0.2 and 1.5 ± 0.1 $s^{-1}$, respectively. The amplitude of the lag phase observed in the CaM:DRE29 complex accounted for ~22% of the signal change with a $k_{off}$ of 8.3 ± 3.5 $s^{-1}$. The dissociation of $Ca^{2+}$ from CaM and CaMRR2 as well as CaM:DRE29 and CaMRR2:DREAM complexes was measured in the temperature range of 6.5−24.7 °C, and the decay times are listed in Table S1 of the Supporting Information. Analysis of the dissociation rates as a function of temperature using Eyring plots[44] shows a larger contribution of the enthalpic component to the activation parameters of dissociation of $Ca^{2+}$ from CaM and CaM:DRE29 (Table 1). The activation parameters for $Ca^{2+}$CaM ($\Delta H^{‡}$ = 12.9 ± 0.5 kcal/mol, and $T\Delta S^{‡}$ = −3.5 ± 0.5 kcal/mol) and the fast phase of $Ca^{2+}$CaM:DRE29 ($\Delta H^{‡}$ = 13.8 ± 0.4 kcal/mol, and $T\Delta S^{‡}$ = −2.7 ± 0.2 kcal/mol) are identical and likely correspond to the same process. On the other hand, $Ca^{2+}$ dissociation activation parameters for CaMRR2 show enthalpy and entropy contributions of 8.6 ± 0.6 and −8.6 ± 0.6 kcal/mol, respectively. The slow phase of $Ca^{2+}$ dissociation observed in the presence of the DRE29 peptide also shows a large enthalpy barrier with a $\Delta H^{‡}$ of 16.1 ± 0.3 kcal/mol and a $T\Delta S^{‡}$ of −1.1 ± 0.2 kcal/mol. In the presence of the full-length DREAM protein, the kinetics of dissociation from CaMRR2 were not significantly different (Table 1) from those in the absence of DREAM. Therefore, the recovered CaMRR2 activation parameters likely



DOI: 10.1021/acs.biochem.5b00251
*Biochemistry* 2015, 54, 4391−4403

arise from a combination of $Ca^{2+}$ and protein dissociation activation barriers. The protein dissociation activation parameters can be approximated by subtracting the activation barrier for CaMRR2 from those of CaMRR2:DREAM, which result in a $\Delta H^{\ddagger}$ of 4.9 ± 0.5 kcal/mol and a $T\Delta S^{\ddagger}$ of 4.6 ± 0.8 kcal/mol. These results show that the core domain of DREAM facilitates the dissociation of residues 29−44 from CaMRR2 by lowering the enthalpic dissociation activation barrier.

**The DREAM:CaM Protein Complex Forms a Nearly Spherical Heterotetramer.** We employed time-resolved fluorescence anisotropy decay to recover the rotational correlation time of calmodulin and DRE29 as well as the CaM:DREAM complex. Fluorescence emission spectra and fluorescence lifetime decay of FITC-labeled DREAM(29−44) show no changes upon binding of calmodulin. Analysis of the frequency domain fluorescence decay using a Gaussian model yields satisfactory fits for the DRE29 peptide and CaM:DRE29 complex (decay parameters listed in Table 2). A bimodal model was necessary to accurately fit the anisotropy decay data, and the recovered rotational correlation times for the CaM:DRE29 complex are listed in Table 3. The fast rotational correlation time of 0.57 ns for DRE29 accounts for 57% of the depolarization and can be attributed to a local motion of the fluorophore. The second rotational correlation time of 2.0 ns for the DRE29 peptide is ∼2-fold larger than that expected for a spherical peptide of 1.0 ns, calculated using the Einstein−Stokes equation (2.6 kDa and 0.3 mL/g hydration).[45] The CaM:DRE29 complex shows a similar local rotational time of 0.61 ns, while the global motion time increased to 10.8 ns. The expected rotational time of a sphere with a molecular weight similar to that of the CaM:DRE29 complex (19 kDa and 0.30 mL/g hydration) yields a rotational diffusion time of 8.0 ns. The discrepancies observed could be due to deviations from a spherical conformation and/or a higher level of protein hydration. These results show that CaM binds to DRE29 as a monomer to form a complex with nearly spherical shape, likely similar to the often observed wraparound conformation of CaM:peptide complexes.[46]

**Table 2. Photophysical Properties of DRE29 and CaM-IAEDANS upon Complex Formation**[a]

| | $r_{ss}$ | $\lambda_{max}$ (nm) | $\tau_1$ (ns) | $\alpha_1$ (%) | $\tau_2$ (ns) | $\alpha_2$ (%) | $\chi^2$ |
|---|---|---|---|---|---|---|---|
| DRE29[b] | 0.010 | 517 | 3.6 | | | | 1.0 |
| DRE29:CaM[b] | 0.090 | 516 | 3.9 | | | | 0.7 |
| IAEDANS | 0.006 | 505 | 4.1 | 14 | 10.5 | 86 | 1.7 |
| apoCaM | 0.049 | 495 | 10.8 | 80 | 16.9 | 20 | 1.1 |
| $Ca^{2+}$CaM | 0.081 | 484 | 10.6 | 55 | 18.9 | 45 | 1.3 |
| apoCaM:DREAM | 0.113 | 486 | 10.6 | 89 | 21.1 | 11 | 0.9 |
| $Ca^{2+}$CaM:DREAM | 0.132 | 475 | 11.3 | 51 | 21.9 | 49 | 0.9 |

[a]Recovered parameters from global analysis of at least three independent measurements of the phase delay and modulation ratio using a Gaussian or double-exponential decay model. The lifetime parameters ($\tau_1$ and $\tau_2$) were set as linked variables and the pre-exponential parameters ($\alpha_1$ and $\alpha_2$) as free variables; $\chi^2$ represents the goodness of fit. [b]A Gaussian lifetime distribution was used, with a recovered width of 0.5 ns for DRE29 and 1.0 ns for the DRE29:CaM complex. Sample concentrations were 0.5 μM DRE29 and 10 μM CaM or 10 μM CaM-IAEDANS and 20 μM DREAM.

To investigate the oligomerization state of calmodulin bound to full-length DREAM, we employed a fluorescently labeled CaM-IAEDANS construct. The long fluorescence lifetime decay and solvent sensitivity of IAEDANS allow us to resolve slower correlation times as well as changes in the probe environment.[47] The fluorescence emission spectra of CaM-IAEDANS upon calcium binding show an increase in fluorescence and a blue shift from 495 to 484 nm (Figure 6a). A modest increase in the steady-state anisotropy can be observed upon binding of $Ca^{2+}$ to CaM-IAEDANS, from an $r_{ss}$ of 0.049 to an $r_{ss}$ of 0.081. Additional information is obtained from lifetime measurements, which show a small increase in lifetime from 16.9 ns for apoCaM to 18.9 ns for $Ca^{2+}$-bound CaM and a change in pre-exponential factor $\alpha_2$ of 25%, likely due to a decrease in the solvent accessibility of the probe (Table 1). Analysis of the $\chi^2$ surface of the phase/modulation fits also reveals that in the absence of $Ca^{2+}$, the C-terminal domain of CaM is more heterogeneous and solvent-exposed based on the smaller $\tau_2$ (Figure 6b). The rotational correlation times recovered from the fit of the anisotropy decay yield values of 0.51 and 0.64 ns for the local motion of IAEDANS attached to apo and calcium-bound CaM, respectively, and 6.7 and 8.1 ns for the global motion of apo and calcium-bound CaM, respectively. The increase in $\theta_1$ is significant (Figure 6c) and correlates with a decrease in the local flexibility of the Cys148 region. On the other hand, the increase in $\theta_2$ upon $Ca^{2+}$ binding is likely due to a more rigid and elongated structure of $Ca^{2+}$CaM in solution. Nonetheless, the rotational correlation times are in good agreement with the expected rotational time for CaM-IAEDANS of 7.1 ns (17.2 kDa and 0.3 mL/g hydration). Overall, these results indicate that association of calcium induces the region near Cys148 to become less flexible and solvent-restricted, which is in good agreement with the rearrangement of CaM structure upon $Ca^{2+}$ binding.[4,48]

We also investigated the effects of association of CaM-IAEDANS with DREAM and found that the emission of $Ca^{2+}$-bound CaM-IAEDANS increases 2-fold upon addition of DREAM with a maximum at 475 nm (Figure 6a). A small increase in intensity and a blue shift to 486 nm were also observed for apoCaM-IAEDANS in the presence of DREAM.

**Table 3. Anisotropy Decay Parameters of DRE29 and CaM-IAEDANS upon Complex Formation**[a]

| | $\theta_1$ (ns) | $f_1$ | $\theta_2$ (ns) | $f_2$ | $\theta_3$ (ns) | $f_3$ | $\chi^2$ |
|---|---|---|---|---|---|---|---|
| DRE29 | 0.57 | 0.72 | 2.0 | 0.28 | | | |
| $Ca^{2+}$CaM:DRE29 | 0.61 | 0.42 | 10.8 | 0.58 | | | 0.6 |
| apoCaM | 0.51 | 0.80 | 6.7 | 0.20 | | | 1.0 |
| $Ca^{2+}$CaM | 0.64 | 0.52 | 8.1 | 0.48 | | | 0.7 |
| apoCaM:DREAM | 0.59 | 0.79 | 8.1 | 0.20 | 56 | 0.01 | 0.7 |
| $Ca^{2+}$CaM:DREAM | 0.62 | 0.31 | 8.9 | 0.31 | 47 | 0.38 | 0.8 |

[a]Recovered from global analysis of at least three independent measurements of the phase and modulation data using a double-exponential decay model. Decay parameters ($\theta_1$−$\theta_3$) were set as linked variables, and the fractional depolarizations ($f_1$−$f_3$) were set as free variables. $\chi^2$ represents the goodness of fit. Sample conditions are identical to those listed for Table 2.



DOI: 10.1021/acs.biochem.5b00251
Biochemistry 2015, 54, 4391−4403

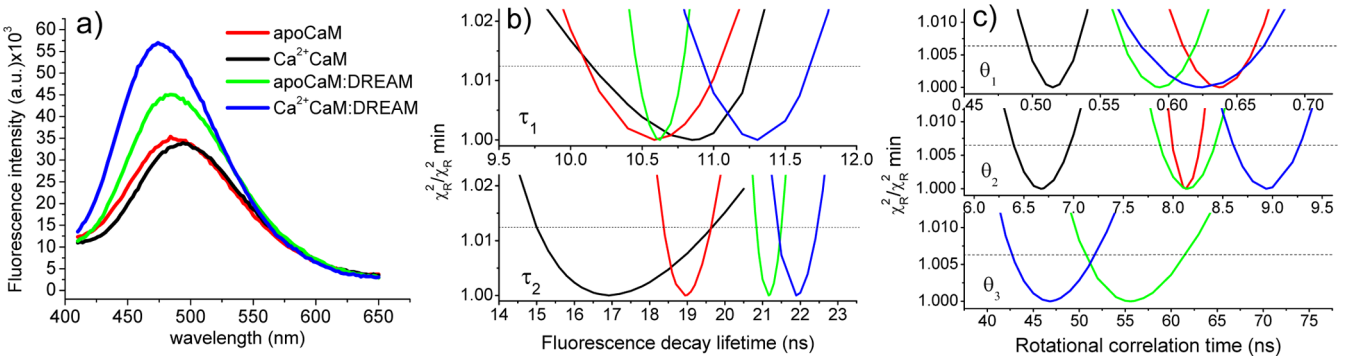


**Figure 6.** (a) Fluorescence emission spectral transition of 5 $\mu$M CaM-IAEDANS upon association with 20 $\mu$M DREAM. (b) Global fluorescence decay lifetime $\chi^2$ surface for the two-component exponential decay of CaM-IAEDANS in the presence (red) or absence (black) of $Ca^{2+}$ and $Ca^{2+}$CaM-IAEDANS:DREAM (blue) and the $Ca^{2+}$ free complex (green). Rotational correlation time $\chi^2$ surface from the global analysis of the anisotropy decay data using a two-component exponential decay for CaM-IAEDANS and triple-exponential decay model for the CaM-IAEDANS:DREAM complex, following the color scheme in panel b.

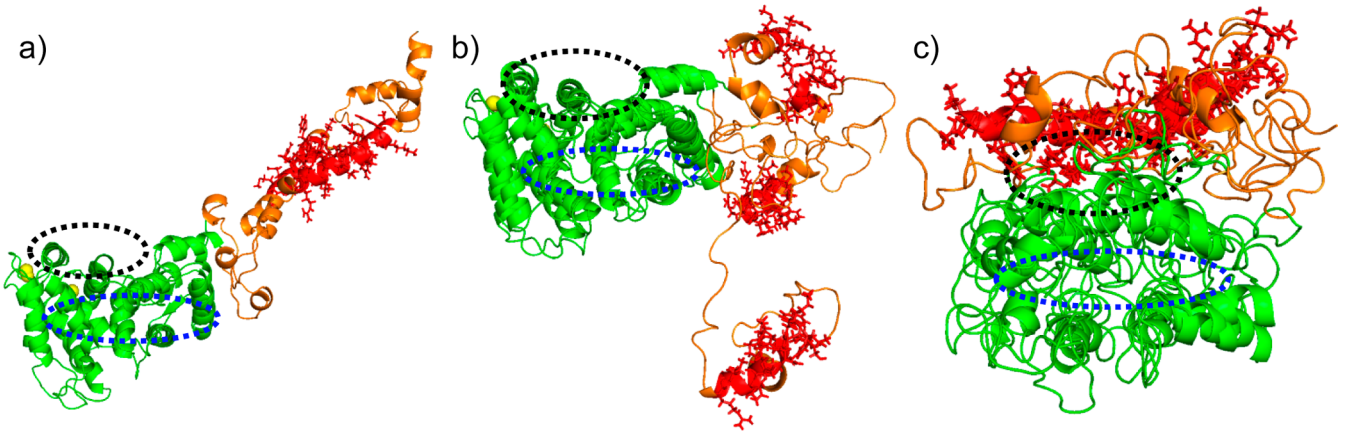


**Figure 7.** Molecular dynamics simulation of DREAM using an initial model constructed by combining a peptide model for residues 1−76 with the published NMR structure of DREAM (residues 76−256) colored green. The $\alpha$-helical section of the N-terminal domain was predicted using secondary prediction tools and is colored orange, and the CaM binding region corresponding to residues 29−44 is shown as red licorice. All structures are aligned using residues 76−256; calcium is shown as yellow spheres. (a) Two final structures of DREAM after 80 ns classical MD simulations. (b) Three final structures of DREAM after 30 ns accelerated MD simulations. (c) Three independent structures of DREAM after 1000 ns of coarse grained molecular dynamics simulation in the absence of $Ca^{2+}$, showing a collapsed N-terminus. The hydrophobic surface known to mediate ligand binding on DREAM is highlighted by a blue ellipse, and the electronegative surface identified in Figure 1 is highlighted in black.

The fluorescence decay lifetime of $Ca^{2+}$CaM-IAEDANS was affected by association with DREAM, showing an increase in the long fluorescence decay lifetime ($\tau_2$) from 18.9 to 21.9 ns. A larger increase in $\tau_2$ was observed for $Ca^{2+}$ free CaM-IAEDANS upon addition of DREAM (from 16.9 to 21.1 ns); however, the amplitude of this decay was ∼4-fold lower than that of the $Ca^{2+}$CaM-IAEDANS:DREAM complex. Further analysis of the fluorescence of CaM-IAEDANS using anisotropy decay shows that in addition to the local and global rotation of apo and $Ca^{2+}$CaM-IAEDANS, a third rotation with correlation times of 56 and 47 ns is present (Figure 6c and Table 3). The rotational correlation time for the $Ca^{2+}$CaM-IAEDANS:DREAM complex is similar to that expected for a spherical CaM:DREAM heterotetramer (calculated value of 40 ns at 0.3 mL/g hydration). The larger rotation for the apoCaM-IAEDANS:DREAM complex could be due to the presence of a mixture of oligomers. Analysis of the $\chi^2$ surface reveals that the rotation of the CaM-IAEDANS:DREAM complex is heterogeneous, ranging from 43 to 52 ns and from 51 to 61 ns in the presence and absence of $Ca^{2+}$, respectively (Figure 6c). Such a heterogeneity likely arises from an extended and flexible conformation of the protein complex. These results indicate that not only the calcium-bound CaM but also the apo form can interact with DREAM, likely with a significantly lower affinity. The solvent accessibility of IAEDANS decreases upon protein complex formation, suggesting that Cys148 forms part of the protein interface. It also supports a model in which a $Ca^{2+}$DREAM dimer associates with two $Ca^{2+}$CaM molecules to form a nearly spherical hetero-tetramer.

**Molecular Dynamics Simulations Support a Model in Which the N-Terminus of DREAM Interacts with an Electrostatic Patch on the Surface of DREAM.** To improve our understanding of the interaction between the N-terminus and the core domain of DREAM, we conducted multiple molecular dynamics simulations using three different strategies (Figure S5 of the Supporting Information). Our initial approach to model the N-terminus of DREAM as an extended domain with partial $\alpha$-helical structure followed by an 80 ns cMD simulation resulted in structures that are shown in Figure 7a. We observed that during the simulation most of the $\alpha$ helices are retained and there is a partial contraction of the structure. The extended conformation of the N-terminus likely arises from insufficient



DOI: 10.1021/acs.biochem.5b00251
*Biochemistry* 2015, 54, 4391−4403

simulation time. To overcome the computational cost of longer cMD simulations, we performed three additional aMDs in which an additional energy was applied to the dihedral angles. This type of simulation results in larger conformational space sampling, and as shown in Figure 7b, the N-terminus of DREAM adopts a more unfolded and collapsed structure. Nonetheless, the CaM binding region is still significantly accessible to solution. Finally, we modeled DREAM using a residue-based coarse grained approach, which significantly decreases computational costs and increases sampling time. In Figure 7c, we show three representative all-atom structures obtained from coarse grained simulations that clearly show a collapse of the N-terminus. Furthermore, all of our simulations resulted in a collapse of the N-terminus near the electronegative surface of DREAM (shown as a black ellipse) and away from the hydrophobic cavity (blue ellipse).

**CaM Modulates the $Ca^{2+}$-Dependent Association of DREAM and DNA.** It has been well reported that DREAM interacts with the DRE promoter sequence of many genes, including *c-fos*, *c-jun*, and *prodynorphin*.[8,12,49] It was proposed that the interaction between DREAM and its target DNA is mediated by basic residues residing on the entering helix of EF-hand 1 (Lys101, Arg98, Lys91, and Lys90) that form an electropositive region at the N-terminus (Figure 1d). Additionally, DREAM-(Δ64) binds DNA with an affinity ~2-fold lower than that of the full-length DREAM.[12] We hypothesize that the presence of numerous basic residues at the N-terminus of DREAM enhances its interaction with DNA and that association with CaM may result in a decrease in DNA binding affinity. We employed a fluorescently labeled dsDNA homologous to the DRE sequence of the human *prodynorphin* gene and monitored the change in fluorescence anisotropy in the presence of DREAM and CaM. As shown in Figure 8, addition of 5 μM DREAM results in a sharp increase in fluorescence anisotropy in the presence or absence of $Ca^{2+}$. Furthermore, upon addition of increasing concentrations of CaM, a decrease in anisotropy is observed, only in the presence of $Ca^{2+}$. Addition of 2 mM EDTA results in the reversal of the CaM-induced decrease in anisotropy, to a value identical to that observed for DREAM in the absence of CaM. These results support the idea that in the presence of the N-terminus, $Ca^{2+}$-bound DREAM interacts with DNA, unless CaM is present to sequester its N-terminal domain.

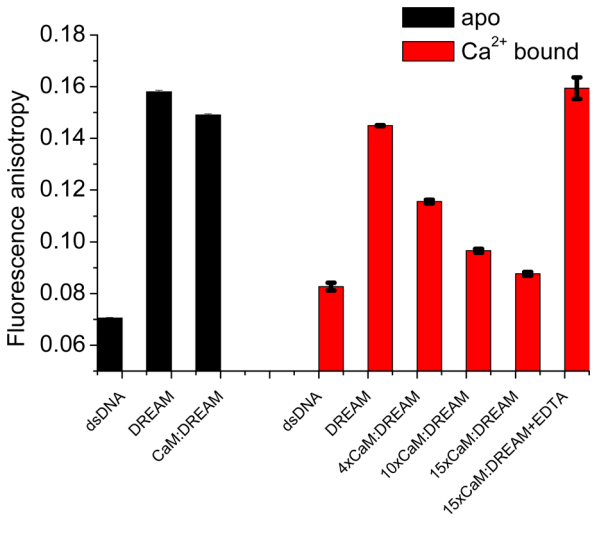


**Figure 8.** Fluorescence anisotropy increase due to 0.5 μM FITC-labeled dsDNA homologous to the DRE sequence of the human *prodynorphin* gene binding to 5 μM DREAM in the presence or absence of $Ca^{2+}$. Addition of CaM at increasing concentrations (0, 20, 40, and 60 μM) results in a concomitant decrease in fluorescence anisotropy. Chelation of $Ca^{2+}$ by 2 mM EDTA results in an increase in anisotropy due to association of dsDNA with DREAM, even in the presence of 60 μM CaM.

## DISCUSSION

The principal goal of this study is to present a model for the interface between the CaM:DREAM protein complex. On the basis of our results, it is clear that residues 29−44 of DREAM associate with CaM in a $Ca^{2+}$-dependent manner with a $K_d$ of ~136 nM. Association of CaM at the N-terminus results in a blue shift and an increase in tryptophan fluorescence on DREAM as well as on the DRE29 peptide, likely due to solvent restriction of Trp32 (Figure 2). The calcium dependency of association of CaM with the DRE29 peptide is similar to that of the intact DREAM protein; however, the affinity is decreased to a $K_d$ of 3.3 ± 0.9 μM. This indicates that the core domain of DREAM (residues comprising helices 1−10) contributes to a decrease in binding energy of ~1.8 kcal/mol. Such a decrease in the free energy of the complex could be due to greater steric hindrance of residues 29−44 in the presence of the rest of the protein or a direct interaction between the N-terminal residues and the core domain of DREAM. Indeed, titration of residues 29−44 with DREAM(Δ64) or DREAM shows the formation of a complex, with a $K_d$ of ~0.3 mM (~−3 kcal/mol). Such a low affinity for the N-terminal domain with the core domain of DREAM is not irrelevant. The local concentration of the N-terminus can be calculated to be ~3 mM, assuming an extended conformation of DREAM of ~100 Å ($0.5 \times 10^{-21}$ L), which would result in approximately 91% of the N-terminus being associated with the core domain of DREAM. However, it is likely that the interaction between DRE29 and DREAM is favored by increased peptide flexibility. Therefore, using a $K_d$ of ~5 mM would be more appropriate (calculated from the decrease in binding energy of 1.8 kcal/mol), which shows that only ~60% of the N-terminal domain is accessible to bind CaM. The collapse of the N-terminus seems to be nonspecific and mainly driven by electrostatic interactions. This conclusion explains why the hydrophobic cavity of DREAM at the C-terminus is not compromised and can bind small hydrophobic ligands such as 1,8-ANS and NS5806 as well as large peptides such as the N-terminus of Kv4.3 (Figure 3). Moreover, the puzzling calcium-independent association of DREAM with Kv4.3 indicates that the N-terminus of DREAM is able to modify the accessibility of the hydrophobic groove. A similar effect was observed for NS5806,[20] and it is possible that the presence of the N-terminus results in a destabilization of the hydrophobic groove that facilitates association with large hydrophobic peptides such as Kv4.3. A calcium-independent binding of KChIPs and Kv4 channels has been observed using full-length proteins.[10,36] However, we and others have reported a calcium-dependent association of KChIP1 (which lacks the extended N-terminal domain) and DREAM(Δ64) with fragments of Kv4.[20,35,50] Therefore, the results presented here support a mechanism in which the presence of the N-terminus in DREAM enhances association with Kv4 channels, whereas its truncation by caspase-3 likely results in disruption of the DREAM:Kv4 complex in the absence of calcium.[17]

Despite the observed flexibility of the N-terminal domain, far- and near-UV CD spectra support a model in which the first 64 residues do not form a random coil, but rather a partial helical


DOI: 10.1021/acs.biochem.5b00251
Biochemistry 2015, 54, 4391−4403

structure. This is supported by bioinformatics analysis that highlights a region of high helical propensity, here named $\alpha_0$ (residues 27−53). Additionally, analysis of the disorder propensity of the DREAM amino acid sequence reveals that the N-terminus is comprised of two disordered regions connected by a structured segment, identified as $\alpha_0$. The N-terminal tryptophans (Trp32 and Trp50) within $\alpha_0$ undergo a structural reorganization upon calcium binding that correlates with an increase in solvent polarity.[41] However, the contribution to the observed near-UV ellipticity change upon $Ca^{2+}$ binding being due the disulfide bond between Cys45 and Cys46 cannot be ruled out.[40,51] We hypothesize that upon $Ca^{2+}$ binding the surface charge reduction on DREAM as well as structural rearrangements may lead to a decrease in the collapse of the N-terminus, thus inducing an increase in the level of solvent exposure of the N-terminus. Near-UV data also do not support a model in which the N-terminus collapses into the hydrophobic cavity, which would result in a reversal of the observed transition.

As seen for other CaM binding peptides, the association between CaM and the N-terminus of DREAM is fast and close to the diffusion limit.[42,43] On the other hand, dissociation of CaM from DRE29 proceeds only after dissociation of $Ca^{2+}$ from CaM. Whether the dissociation requires dissociation of all $Ca^{2+}$ ions or only those at the CaM C-terminal domain is not revealed by these experiments. However, the observed displacement of the DRE29 peptide by TFP bound at the C-terminus highlights the possibility that this domain plays a major role in complex formation. The change in fluorescence anisotropy upon dissociation of $Ca^{2+}$ from CaMRR2 shows kinetics much slower than that observed using tyrosine residues located in the C-terminal domain. The position of the rhodamine label at the C-terminus on the exiting helix of EF-4 near the hydrophobic pocket may allow the xanthene group to stabilize the open conformation, which results in a much slower transition of CaM to the closed apo form. Furthermore, the temperature dependence of the dissociation kinetics allows us to extract the activation enthalpy and entropy for the dissociation of DRE29 and DREAM from apoCaM. These thermodynamic parameters reveal that the presence of the core domain of DREAM resulted in an enthalpy of activation (4.9 kcal/mol) approximately 3-fold lower than that of dissociation of DRE29 (16.1 kcal/mol). We hypothesize that this difference arises from an electrostatic attraction of the N-terminal domain involved in binding of CaM to the electronegative side of DREAM (Figure 1). On the other hand, the positive 4.0 kcal/mol activation entropy for dissociation of CaMRR2 from DREAM compared to −1.1 kcal/mol for the DRE29 dissociation shows that the dissociation transition states are not identical. These results support our hypothesis that there is an electrostatic interaction between the N-terminal domain and the core domain of DREAM, as well as the idea that CaM decreases the level of disorder of the N-terminus, which likely explains the increase in the solubility of DREAM.

DREAM has been shown to undergo an oligomerization change upon binding of calcium; however, there seems to be some disagreement among the reported oligomerization states. We have recently reported that in the absence of calcium, the DREAM(Δ64) construct forms a stable tetramer in solution and a dimer upon calcium binding.[29] In contrast, Ramachandran and co-workers observed a dimer to monomer transition upon calcium binding to DREAM,[13] which is contrary to the initial finding favoring a tetramer to dimer transition.[14] The disagreement could be likely due to different expression methodologies (GST fusion vs inclusion body refolding), and/or sample conditions (high salt vs low salt and 10 mM LDAO). Therefore, to understand the impact of association of CaM with DREAM, we determined the structural arrangement and oligomerization of CaM:DRE29 and CaM:DREAM complexes using steady-state and time-resolved spectroscopy.

The fluorescence properties of the IAEDANS-labeled CaM show a clear transition upon $Ca^{2+}$ binding, which include an increase in fluorescence, a blue shift in emission, and a slower decay lifetime and rotational correlation time of the protein. These results are in good agreement with the known transition of CaM from a flexible conformation in the apo form to a more rigid and elongated structure in the presence of calcium with concomitant exposure of a hydrophobic surface at the C-terminus.[4,48] Association of CaM-IAEDANS with DREAM results in an even more dramatic increased fluorescence, a larger blue shift, and an increased decay lifetime as well as a more complex rotational decay. Noticeably, CaM and DRE29 form a spherical heterodimer whereas a heterotetramer was observed for the CaM-IAEDANS:DREAM complex, which supports a stoichiometry of 1:1. Moreover, the fact that $Ca^{2+}$DREAM forms a dimer in the presence of CaM supports the idea that CaM association does not disrupt the dimer interface that is partially solvent protected in calcium-bound DREAM dimer[15] and likely does not affect the accessibility of the hydrophobic groove on DREAM or its interaction with hydrophobic partners.[15,20,29]

Multiple simulations of a DREAM model derived from bioinformatics analysis (Figure 7) show that the N-terminus of DREAM likely collapses on a negative surface adjacent to the hydrophobic surface. The interaction between the core domain and the N-terminus of DREAM is mainly mediated by Asp and Glu residues on the exiting helix of EF-2 and EE-4 and entering helix of EF-3 as well as on the loop of EF-4. The position of the N-terminus also does not conflict with the proposed structure of KChIPs bound to the T1 domain of Kv4 channels.[36,52] It is well-known that the drosophila shaker channels (homologous to Kv4 in humans) can inactivate through pore occlusion mediated by a long and flexible positively charged N-terminus.[53] The positive charge and conformational flexibility of the N-terminal domain of DREAM could highlight the role of this domain in modulation of Kv4 channels through a mechanism similar to that of shaker channels. Moreover, the divergent amino acid sequence among the KChIP subfamily of $Ca^{2+}$ binding proteins could explain the observed variation in modulation of $K^+$ currents by KChIPs.

Finally, binding of CaM to DREAM shows a clear effect on the interactions of DREAM with the DRE sequence of the prodynorphin gene, an effect that likely translates to other DRE-promoted genes regulated by DREAM.[49] Our observation that DREAM associates with DNA independent of calcium is in contrast to previous work.[12] However, we believe that the discrepancy arises from different experimental conditions since previous ITC experiments were conducted in the presence of LDAO. We observed that both LDAO and CaM increase the solubility of DREAM, and it is possible that association of LDAO with DREAM modulates the interactions between DRE and DREAM and potentially inhibits the interaction between $Ca^{2+}$DREAM and DNA. Indeed, we have observed inhibition of the CaM:DREAM interaction by LDAO as well as a strong interaction between DRE29 peptide and DRE dsDNA with LDAO (data not shown). The $EC_{50}$ for $Ca^{2+}$CaM-induced DREAM DNA dissociation observed here is relatively high, ∼20 μM. However, the high intracellular concentrations of CaM, the



DOI: 10.1021/acs.biochem.5b00251
Biochemistry 2015, 54, 4391−4403

known $Ca^{2+}$-induced translocation of CaM from the cytosol to the nucleus, and the $Ca^{2+}$-induced increase in the freely diffusing CaM concentration could facilitate the formation of the DREAM:CAM complex and dissociation of DREAM from DNA.[54,55] It is also possible that post-translational modification such as myristoylation/palmytoylation at Cys45/Cys46 could enhance the affinity between CaM and DREAM and decrease the observed $EC_{50}$, an effect that has been observed in other CaM binding proteins.[56]

## CONCLUSION

We have shown that an $\alpha$-helical region at the N-terminus of DREAM comprising residues 29−44 contains a CaM binding surface. The $Ca^{2+}$-dependent association of CaM with DREAM increases its solubility in the presence of calcium. We also demonstrate that the N-terminus of DREAM forms a flexible $Ca^{2+}$ sensitive domain, which can collapse on the core domain of DREAM but does not block the hydrophobic cavity at the C-terminus. The protein complexes between CaM and DRE29 or DREAM follow a 1:1 stoichiometry, in good agreement with a heterodimer and heterotetramer oligomerization. Overall, our biochemical studies provide insight into the molecular mechanism of the CaM:DREAM complex and the impact of association of CaM with DREAM and open the possibility of the CaM:DREAM complex being involved in gene regulation. The complex behavior of the N-terminus in DREAM highlights the functional diversity of members of the KChIPs group of calcium binding proteins, which share a low degree of homology in this region. These results also provide a roadmap for the design of a molecular model of the CaM:DREAM complex, which may shed light on the understanding of these multifunctional proteins and how they affect downstream binding partners such as Kv4 channels, DNA, and presenilin.

## ASSOCIATED CONTENT

### Supporting Information

Additional experimental results, including the dissociation kinetics between CaM:DRE29 and CaMRR2:DREAM, the determined association constant between CaMRR2 and DRE29, the effect of ionic strength on binding of DRE29 to the core domain of DREAM, structures of the N-terminal domain of DREAM after MD simulations and full-length DREAM before MD simulations, and phase delay and modulation ratios of the fluorescence decay and anisotropy decay of CaM-IAEDANS complexes. The Supporting Information is available free of charge on the ACS Publications website at DOI: 10.1021/acs.biochem.5b00251.

## AUTHOR INFORMATION

### Corresponding Author

*Department of Chemistry and Biochemistry, Florida International University, 11200 SW 8th St., Miami, FL 33199. Phone: 305-348-7406. Fax: 305-348-3772. E-mail: miksovsk@fiu.edu.

### Funding

This work was supported by the National Science Foundation (MCB 1021831, J.M.). W.G.G. and A.S.A. were partially funded by National Institute of General Medical Sciences Grant R25 GM061347.

### Notes

The authors declare no competing financial interest.

## ABBREVIATIONS

DREAM, downstream regulatory element antagonist modulator; CaM, calmodulin; KChIP, potassium channel interacting protein; DREAM(Δ64), mouse DREAM construct lacking residues 1−64; DRE29, DREAM peptide residues 29−44; DRE, downstream regulatory element; EF-*X*, EF-hand *X*; 1,8-ANS, 8-anilinonaphthalene-1-sulfonic acid; CD, circular dichroism.

## REFERENCES

(1) Carafoli, E. (2002) Calcium signaling: A tale for all seasons. *Proc. Natl. Acad. Sci. U. S. A. 99*, 1115−1122.
(2) Clapham, D. E. (2007) Calcium signaling. *Cell 131*, 1047−1058.
(3) Crivici, A., and Ikura, M. (1995) Molecular and structural basis of target recognition by calmodulin. *Annu. Rev. Biophys. Biomol. Struct. 24*, 85−116.
(4) Chattopadhyaya, R., Meador, W. E., Means, A. R., and Quiocho, F. A. (1992) Calmodulin structure refined at 1.7 Å resolution. *J. Mol. Biol. 228*, 1177−1192.
(5) Zhang, M., Tanaka, T., and Ikura, M. (1995) Calcium-induced conformational transition revealed by the solution structure of apo calmodulin. *Nat. Struct. Biol. 2*, 758−767.
(6) Rhoads, A. R., and Friedberg, F. (1997) Sequence motifs for calmodulin recognition. *FASEB J. 11*, 331−340.
(7) Chin, D., and Means, A. R. (2000) Calmodulin: A prototypical calcium sensor. *Trends Cell Biol. 10*, 322−328.
(8) Naranjo, J. R., Carrión, A. M., Link, W. A., Ledo, F., and Mellstrom, B. (1999) DREAM is a $Ca^{2+}$-regulated transcriptional repressor. *Nature 398*, 80−84.
(9) Buxbaum, J. D., Choi, E., Luo, Y., Lilliehook, C., Crowley, A. C., Merriam, D. E., and Wasco, W. (1998) Calsenilin: A calcium-binding protein that interacts with the presenilins and regulates the levels of a presenilin fragment. *Nat. Med. 4*, 1177−1181.
(10) An, W. F., Bowlby, M. R., Betty, M., Cao, J., Ling, H., Mendoza, G., Hinson, J. W., Mattsson, K. I., Strassle, B. W., Trimmer, J. S., and Rhodes, K. J. (2000) Modulation of A-type potassium channels by a family of calcium sensors. *Nature 403*, 553−556.
(11) Burgoyne, R. D., and Weiss, J. L. (2000) The neuronal calcium sensor family of $Ca^{2+}$-binding proteins. *Biochem. J. 353*, 1−12.
(12) Osawa, M., Dace, A., Tong, K. I., Valiveti, A., Ikura, M., and Ames, J. B. (2005) $Mg^{2+}$ and $Ca^{2+}$ differentially regulate DNA binding and dimerization of DREAM. *J. Biol. Chem. 280*, 18008−18014.
(13) Ramachandran, P. L., Craig, T. A., Atanasova, E. A., Cui, G., Owen, B. A., Bergen, H. R., Mer, G., and Kumar, R. (2012) The potassium channel interacting protein 3 (DREAM/KChIP3) heterodimerizes with and regulates calmodulin function. *J. Biol. Chem. 287*, 39439−39448.
(14) Osawa, M., Tong, K. I., Lilliehook, C., Wasco, W., Buxbaum, J. D., Cheng, H. -. M., Penninger, J. M., Ikura, M., and Ames, J. B. (2001) Calcium-regulated DNA binding and oligomerization of the neuronal calcium-sensing protein, Calsenilin/DREAM/KChIP3. *J. Biol. Chem. 276*, 41005−41013.
(15) Lusin, J. D., Vanarotti, M., Li, C., Valiveti, A., and Ames, J. B. (2008) NMR structure of DREAM: Implications for $Ca^{2+}$-dependent DNA binding and protein dimerization. *Biochemistry 47*, 2252−2264.
(16) Yu, L., Sun, C., Mendoza, R., Wang, J., Matayoshi, E. D., Hebert, E., Pereda-Lopez, A., Hajduk, P. J., and Olejniczak, E. T. (2007) Solution structure and calcium-binding properties of EF-hands 3 and 4 of calsenilin. *Protein Sci. 16*, 2502−2509.
(17) Choi, E. K., Zaidi, N. F., Miller, J. S., Crowley, A. C., Merriam, D. E., Lilliehook, C., Buxbaum, J. D., and Wasco, W. (2001) Calsenilin is a substrate for caspase-3 that preferentially interacts with the familial alzheimer's disease-associated C-terminal fragment of presenilin 2. *J. Biol. Chem. 276*, 19197−19204.
(18) Gonzalez, W. G., Arango, A., and Miksovska J. (2014) Interaction-based analysis of the mechanism by which the extended amphiphilic N-terminus of DREAM mediates calmodulin binding. Abstracts, 66th


DOI: 10.1021/acs.biochem.5b00251
*Biochemistry* 2015, 54, 4391−4403

Southeast Regional Meeting of the American Chemical Society, Nashville, TN, October 16−19, 2014, SERMACS-566.
(19) Gonzalez, W. G., Arango, A. S., and Miksovska, J. (2015) The N-terminal extension of KChIP3 is responsible for KChIP3-calmodulin complex formation. *Biophys. J. 108*, 279a.
(20) Gonzalez, W. G., Pham, K., and Miksovska, J. (2014) Modulation of the voltage-gated potassium channel (Kv4.3) and the auxiliary protein (KChIP3) interactions by the current activator NS5806. *J. Biol. Chem. 289*, 32201−32213.
(21) George, S. E., Su, Z., Fan, D., and Means, A. R. (1993) Calmodulin-cardiac troponin C chimeras. Effects of domain exchange on calcium binding and enzyme activation. *J. Biol. Chem. 268*, 25213−25220.
(22) Hudson, E. N., and Weber, G. (1973) Synthesis and characterization of two fluorescent sulfhydryl reagents. *Biochemistry 12*, 4154−4161.
(23) Beechem, J. M. (1989) A second generation global analysis program for the recovery of complex inhomogeneous fluorescence decay kinetics. *Chem. Phys. Lipids 50*, 237−251.
(24) Phillips, J. C., Braun, R., Wang, W., Gumbart, J., Tajkhorshid, E., Villa, E., Chipot, C., Skeel, R. D., Kale, L., and Schulten, K. (2005) Scalable molecular dynamics with NAMD. *J. Comput. Chem. 26*, 1781−1802.
(25) Brooks, B. R., Bruccoleri, R. E., Olafson, B. D., States, D. J., Swaminathan, S., and Karplus, M. (1983) CHARMM: A program for macromolecular energy, minimization, and dynamics calculations. *J. Comput. Chem. 4*, 187−217.
(26) Humphrey, W., Dalke, A., and Schulten, K. (1996) VMD: Visual molecular dynamics. *J. Mol. Graphics 14*, 33−38.
(27) Essmann, U., Perera, L., Berkowitz, M. L., Darden, T., Lee, H., and Pedersen, L. G. (1995) A smooth particle mesh ewald method. *J. Chem. Phys. 103*, 8577−8593.
(28) Marrink, S. J., Risselada, H. J., Yefimov, S., Tieleman, D. P., and de Vries, A. H. (2007) The MARTINI force field: coarse grained model for biomolecular simulations. *J. Phys. Chem. B 111*, 7812−7824.
(29) Gonzalez, W. G., and Miksovska, J. (2014) Application of ANS fluorescent probes to identify hydrophobic sites on the surface of DREAM. *Biochim. Biophys. Acta, Proteins Proteomics 1844*, 1472−1480.
(30) Levin, R. M., and Weiss, B. (1977) Binding of trifluoperazine to the calcium-dependent activator of cyclic nucleotide phosphodiesterase. *Mol. Pharmacol. 13*, 690−697.
(31) Cook, W. J., Walter, L. J., and Walter, M. R. (1994) Drug binding by calmodulin: Crystal structure of a calmodulin-trifluoperazine complex. *Biochemistry 33*, 15259−15265.
(32) Pham, K., Dhulipala, G., Gonzalez, W. G., Gerstman, B. S., Regmi, C., Chapagain, P. P., and Miksovska, J. (2015) $Ca^{2+}$ and $Mg^{2+}$ modulate conformational dynamics and stability of downstream regulatory element antagonist modulator. *Protein Sci. 24*, 741−751.
(33) Liang, P., Wang, H., Chen, H., Cui, Y., Gu, L., Chai, J., and Wang, K. (2009) Structural insights into KChIP4a modulation of Kv4.3 inactivation. *J. Biol. Chem. 284*, 4960−4967.
(34) Reddy, P. P., Raghuram, V., Hradsky, J., Spilker, C., Chakraborty, A., Sharma, Y., Mikhaylova, M., and Kreutz, M. R. (2014) Molecular dynamics of the neuronal EF-hand $Ca^{2+}$-sensor caldendrin. *PLoS One 9*, e103186.
(35) Li, M., Lei, L., Jia, L., Ling, X., Zhang, J., Zhao, Y., and Wang, K. (2014) Interactions of KChIP4a and its mutants with Ca2+ or Kv4.3 N-terminus by affinity capillary electrophoresis. *Anal. Biochem. 449*, 99−105.
(36) Pioletti, M., Findeisen, F., Hura, G. L., Minor, and Daniel, L. (2006) Three-dimensional structure of the KChIP1-Kv4.3 T1 complex reveals a cross-shaped octamer. *Nat. Struct. Mol. Biol. 13*, 987−995.
(37) Xue, B., Dunbrack, R. L., Williams, R. W., Dunker, A. K., and Uversky, V. N. (2010) PONDR-FIT: A meta-predictor of intrinsically disordered amino acids. *Biochim. Biophys. Acta, Proteins Proteomics 1804*, 996−1010.
(38) Obradovic, Z., Peng, K., Vucetic, S., Radivojac, P., Brown, C. J., and Dunker, A. K. (2003) Predicting intrinsic disorder from amino acid sequence. *Proteins: Struct., Funct., Genet. 53*, 566−572.
(39) Strickland, E. H. (1974) Aromatic contributions to circular dichroism spectra of proteins. *Crit. Rev. Biochem. Mol. Biol. 2*, 113−175.
(40) Woody, R. W. (2012) Electronic Circular Dichroism of Proteins. In *Comprehensive Chiroptical Spectroscopy*, 2nd ed., pp 473−497, John Wiley & Sons, Inc., Hoboken, NJ.
(41) Nagai, M., Nagatomo, S., Nagai, Y., Ohkubo, K., Imai, K., and Kitagawa, T. (2012) Near-UV circular dichroism and UV resonance raman spectra of individual tryptophan residues in human hemoglobin and their changes upon the quaternary structure transition. *Biochemistry 51*, 5932−5941.
(42) Brown, S. E., Martin, S. R., and Bayley, P. M. (1997) Kinetic control of the dissociation pathway of calmodulin-peptide complexes. *J. Biol. Chem. 272*, 3389−3397.
(43) Kasturi, R., Vasulka, C., and Johnson, J. D. (1993) $Ca^{2+}$, caldesmon, and myosin light chain kinase exchange with calmodulin. *J. Biol. Chem. 268*, 7958−7964.
(44) Eyring, H. (1935) The activated complex in chemical reactions. *J. Chem. Phys. 3*, 107−115.
(45) Einstein, A. (1905) Über die von der molekularkinetischen theorie der wärme geforderte bewegung von in ruhenden flüssigkeiten suspendierten teilchen. *Ann. Phys. 322*, 549−560.
(46) Yamniuk, A., and Vogel, H. (2004) Calmodulin's flexibility allows for promiscuity in its interactions with target proteins and peptides. *Mol. Biotechnol. 27*, 33−57.
(47) Hudson, E. N., and Weber, G. (1973) Synthesis and characterization of two fluorescent sulfhydryl reagents. *Biochemistry 12*, 4154−4161.
(48) Kuboniwa, H., Tjandra, N., Grzesiek, S., Ren, H., Klee, C. B., and Bax, A. (1995) Solution structure of calcium-free calmodulin. *Nat. Struct. Biol. 2*, 768−776.
(49) Ledo, F., Link, W. A., Carrión, A. M., Echeverria, V., Mellström, B., and Naranjo, J. R. (2000) The DREAM−DRE interaction: Key nucleotides and dominant negative mutants. *Biochim. Biophys. Acta, Mol. Cell Res. 1498*, 162−168.
(50) Gonzalez, W., and Miksovska, J. (2013) Modulation of the KV4.3-KchIP3 interactions by $Ca^{2+}$ and NS5806. *Biophys. J. 104*, 102a.
(51) Kelly, S. M., Jess, T. J., and Price, N. C. (2005) How to study proteins by circular dichroism. *Biochim. Biophys. Acta, Proteins Proteomics 1751*, 119−139.
(52) Wang, H., Yan, Y., Liu, Q., Huang, Y., Shen, Y., Chen, L., Chen, Y., Yang, Q., Hao, Q., Wang, K., and Chai, J. (2007) Structural basis for modulation of Kv4 K+ channels by auxiliary KChIP subunits. *Nat. Neurosci. 10*, 32−39.
(53) Antz, C., Geyer, M., Fakler, B., Schott, M. K., Guy, H. R., Frank, R., Ruppersberg, J. P., and Kalbitzer, H. R. (1997) NMR structure of inactivation gates from mammalian voltage-dependent potassium channels. *Nature 385*, 272−275.
(54) Deisseroth, K., Heist, E. K., and Tsien, R. W. (1998) Translocation of calmodulin to the nucleus supports CREB phosphorylation in hippocampal neurons. *Nature 392*, 198−202.
(55) Zaidi, N. F., Thomson, E. E., Choi, E., Buxbaum, J. D., and Wasco, W. (2004) Intracellular calcium modulates the nuclear translocation of calsenilin. *J. Neurochem. 89*, 593−601.
(56) Takasaki, A., Hayashi, N., Matsubara, M., Yamauchi, E., and Taniguchi, H. (1999) Identification of the calmodulin-binding domain of neuron-specific protein kinase C substrate protein CAP-22/NAP-22. direct involvement of protein myristoylation in calmodulin-target protein interaction. *J. Biol. Chem. 274*, 11848−11853.
(57) Baker, N. A., Sept, D., Joseph, S., Holst, M. J., and McCammon, J. A. (2001) Electrostatics of nanosystems: Application to microtubules and the ribosome. *Proc. Natl. Acad. Sci. U. S. A. 98*, 10037−10041.


DOI: 10.1021/acs.biochem.5b00251
*Biochemistry* 2015, 54, 4391−4403